Liquid Phase Exfoliation of Chemically Prelithiated Bilayered Vanadium Oxide in Aqueous Media for Li-ion Batteries

Raymond Zhang¹, Timofey Averianov¹, Ryan Andris¹, Michael J. Zachman², Ekaterina Pomerantseva^{1*}

Keywords: bilayered vanadium oxide; liquid phase exfoliation; nanoflakes; structural water; Liion batteries

Abstract

Bilayered vanadium oxides are attractive for energy storage due to their high initial specific capacities, which could be stabilized by integrating the bilayers with conductive nanoflakes often produced in a form of aqueous dispersions. Therefore, exfoliation of the bilayered vanadium oxides in water with high yield is desirable. This work introduces the first aqueous exfoliation of chemically prelithiated bilayered vanadium oxide (i.e., δ -Li_xV₂O₅·nH₂O or LVO) followed by vacuum filtration to produce a free-standing film, exhibiting a lamellar stacking of the bilayered vanadium oxide nanoflakes as evidenced by scanning electron microscopy. Due to the hydrated nature of bilayered vanadium oxides, the relationship between interlayer water content and the vacuum drying temperature (105°C vs. 200°C) was studied using X-ray diffraction, thermogravimetric analysis, and Raman spectroscopy. It was found that vacuum drying the LVO nanoflakes at 200°C enabled more efficient removal of crystallographic water than drying at 105°C, and without inducing a phase transformation. Scanning transmission electron microscopy confirmed the layered structure of the samples, which was more well-ordered in the 200°C case and had no clear boundaries between flakes at the atomic scale. Furthermore, electrochemical testing in non-aqueous Li-ion cells revealed that vacuum drying at 200°C led to improvements in ion storage capacity and electrochemical stability. Improvements in electrochemical charge storage properties of the electrodes obtained via LVO exfoliation and free-standing film assembly in water dried at 200°C reveal that conventional battery electrode drying protocols need to be revised as new electrochemically active materials are synthesized, such as hydrated layered oxides

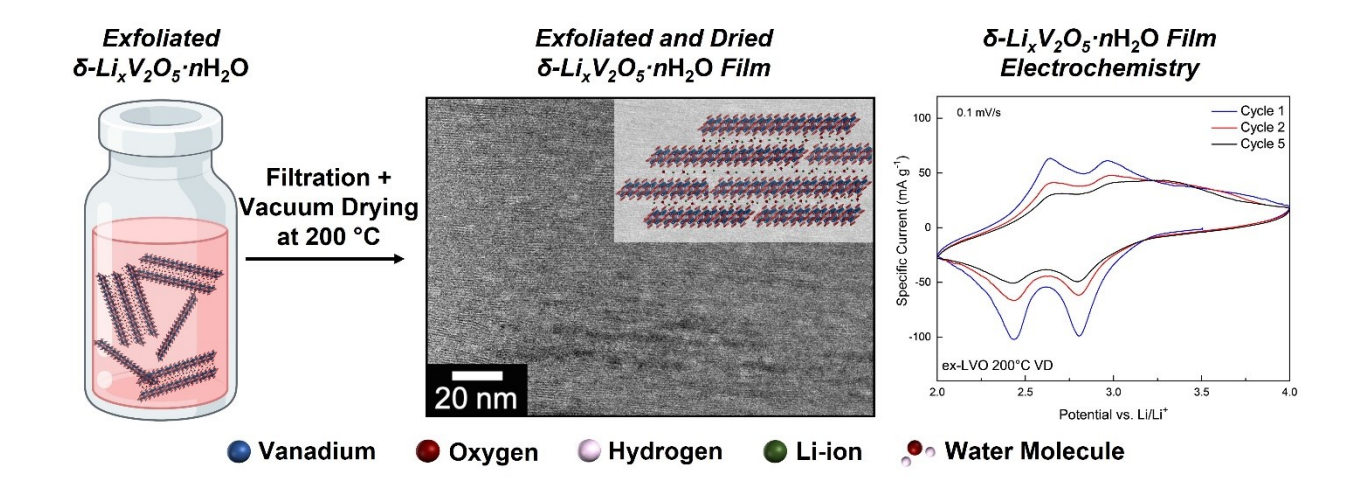
¹ Materials Electrochemistry Group, Department of Materials Science and Engineering, Drexel University, Philadelphia, PA 19104, USA

² Center for Nanophase Materials Sciences, Oak Ridge National Laboratory, Oak Ridge, TN 37831, USA

^{*} Corresponding Author: ep423@drexel.edu

with expanded interlayer regions. The remaining capacity fading can be attributed to the structural LVO degradation, dissolution of vanadium oxide in electrolyte, and parasitic effects of the remaining interlayer water molecules. Our results establish an environmentally friendly and safe approach to obtaining two-dimensional (2D) bilayered vanadium oxide nanoflakes and creates a pathway to constructing novel 2D heterostructures for improved performance in energy storage applications.

Graphical Abstract



1. Introduction

Inorganic two-dimensional (2D) materials are promising components in applications that rely on redox reactions including ion intercalation, such as electrocatalysis and energy storage. A 2D morphology combined with a layered crystal structure offers open diffusion pathways that improve transport of ions. Stabilized layered phases, such as the chemically preintercalated materials can potentially mitigate structural damage from processes that cause material expansion and contraction. Bilayered vanadium oxide, or δ -V₂O₅·nH₂O or BVO, is of particular interest due to its open layered structure, large interlayer spacings, and vanadium's high oxidation state. These properties allow δ -V₂O₅·nH₂O to intercalate a relatively large number of ions accompanied by multiple reduction steps. However, this phase is limited by its low electronic conductivity and poor electrochemical stability. Therefore, studies have focused on developing methods to combine δ -V₂O₅·nH₂O with more conductive phases such as graphene, carbon nanotubes, and conductive carbon precursors to improve electron transport and stabilize high initial specific capacities.

The efficient strategy used to combine 2D materials with complementary properties is the 'top-down' approach. This method requires the exfoliation of two or more dissimilar materials into few layer nanoflakes followed by lamellar assembly into a single heterostructure. For example, unilamellar MnO₂ nanosheets were combined with graphene monolayers to form high-performing electrodes in Na-ion and Li-ion batteries.8 In addition, MXene and single-layer graphene oxide were mixed and thermally reduced to form an electrochemically active free-standing film.⁹ The assembly process can also be aided by functional groups on the exfoliated surfaces to help control layer sequencing. 10 Each of these methods utilizes liquid phase exfoliation (LPE), where bulk precursors are delaminated into nanoflakes in a liquid solvent. 11 This procedure is most efficient in solvents that weaken the interactions between layers to minimize the energy required for exfoliation and prevent agglomeration of the 2D sheets. 12 Consequently, it is important that the solvent is both an effective medium for exfoliation and miscible with other suspensions for use in heterostructure assembly. In order to demonstrate the versatility of the top-down approach and discover 2D heterostructures with superior energy storage properties, new building blocks (i.e., nanoflakes of individual materials) are needed triggering the development of exfoliation approaches for new layered phases. Additionally, availability of nanoflakes in suspensions or in dry powder form opens ways to build sophisticated electrode architectures using a large portfolio

of manufacturing approaches, such as spin-coating, spray-coating, electrospinning, etc.¹¹ Layered oxides are of particular interest due to their stability and redox activity at high potentials, necessary for good cathode performance. Despite high electrochemical activity, no reports have shown 2D heterostructure assembly using bilayered vanadium oxide nanoflakes, possibly due to the absence of suitable BVO exfoliation approaches.

LPE of δ-V₂O₅·nH₂O preintercalated with Li⁺ ions (i.e., δ-Li_xV₂O₅·nH₂O or LVO) was successfully achieved in *n*-methyl-2-pyrrolidone (NMP).¹³ This approach, followed by vacuum filtration, produced a free-standing film comprised of flexible bilayered vanadium oxide nanosheets; however, the yield was low and insufficient for the detailed electrochemical investigation of the charge storage properties. Additionally, NMP is a known irritant, has a low flash point, and may cause developmental toxicity in humans.¹⁴ Alternatively, water is widely available, safe, and environmentally friendly. Further, common conductive materials and precursors to conductive carbons such as Ti₃C₂T_x MXene, and graphene oxide produce highly concentrated and stable dispersions in water.¹⁵ Therefore, exfoliation of the bilayered vanadium oxide in water with high yields is desirable to enable compatibility with conductive 2D nanoflakes.

Water as an exfoliation media can however pose certain challenges. In the case of hydrated layered materials with expanded interlayer regions, such as the BVO, solvent water molecules can enrich interlayer regions through intercalation and adsorption on the surface of the exfoliated nanoflakes. Excess water in hydrated oxides can be detrimental to electrochemical performance in non-aqueous energy storage systems resulting in limited charge storage and poor cycling stability, possibly due to the poorly reversible LiOH formation. Additionally, loosely bound structural water molecules can dissolve in electrolyte during cycling leading to electrolyte decomposition and a possible interaction with a metallic anode material and the formation of an insulating oxide/hydroxide layer on the anode surface. Therefore, standard dehydration procedures for Liion battery electrode preparation may not be sufficient to remove detrimentally excessive water molecules from the surface and interlayer region of the hydrated layered materials. Further understanding of dehydration processes and effect of the structural water on charge storage properties of hydrated layered compounds in non-aqueous energy storage devices can establish strategies to achieve superior performance of 2D materials and heterostructures.

Here we report a simple LPE approach to obtain a highly concentrated and stable colloidal suspension of LVO nanoflakes using low temperature probe sonication in an aqueous medium. Bulk δ-Li_xV₂O₅·nH₂O powder is dispersed in water before a mechanical shear force is applied through probe sonication to induce exfoliation. Vacuum filtration results in a free-standing film that is comprised of highly lamellar nanoflakes that form a nearly continuous material composed of layers oriented approximately in a single direction. Due to the role of water in parasitic processes with lithium ions and the non-aqueous electrolyte, we investigate the impact of vacuum drying temperatures of 105°C and 200°C on the bilayered vanadium oxide crystallographic structure, water content, oxidation state, and electrochemical performance. Thermogravimetric analysis and X-ray diffraction showed that vacuum drying the LVO at 200°C significantly removed water content from the interlayer region without structural degradation of the LVO. Cathodes composed of LVO nanoflakes vacuum dried at 105°C and 200°C were tested in non-aqueous Li-ion half cells. Galvanostatic life cycle tests at 20 mA·g⁻¹ demonstrated higher ion storage capacity and capacity retention for LVO nanoflake cathodes vacuum dried at 200°C, indicating that vacuum drying at elevated temperatures is a viable processing method for enhancing charge storage and cycling stability. Rate capability testing from 20 to 200 mA·g⁻¹ also showed improved capacities and rate tolerance when returning back to 20 mA·g⁻¹ for LVO nanoflakes dried at 200°C. The cost effective and environmentally safe approach to obtain 2D bilayered vanadium oxide nanoflakes enables the opportunity to design 2D heterostructures for energy storage applications. Furthermore, this work also highlights the importance of controlling water content of hydrated materials to improving performance in non-aqueous energy storage systems. The reported liquid exfoliation method in water opens additional opportunities for aqueous energy storage.²⁰

2. Experimental Methods

Preparation of δ -Li_xV₂O₅·nH₂O Precursor

The synthesis of δ-Li_xV₂O₅·*n*H₂O (LVO) is documented in a previous report.⁴ In brief, LiCl (99% Fischer ScientificTM) was dissolved in 30 mL of 15 wt. % H₂O₂ solution (99% Fischer ScientificTM) under stirring at 25 °C. 500 mg of α-V₂O₅ powder (99% Fischer ScientificTM) was added slowly over 15 min and stirred for 1 hour. Next, the temperature was increased to 60°C and the mixture was stirred for another hour. Subsequently, 1 mL of 30 wt. % H₂O₂ was added and the stirring continued for additional two hours. The resulting precipitate was aged for four days under ambient conditions, then it was washed with DI water using a vacuum filtration apparatus followed by drying at 105°C in air for 24 hours. The dried material was ground into a powder and vacuum dried (VD) at 105°C and 200°C separately for 24 hours. These samples are referred to as LVO precursor 105°C VD and LVO precursor 200°C VD, respectively.

Exfoliation and processing of nanosheets

The LVO powder was exfoliated using a Qsonica Q125 ultrasonic processor with a 3.175 mm diameter probe tip. 200 mg of the powder was added to 10 mL of DI water in a 20 mL vial placed in an ice bath. The suspensions were sonicated for 2 hours at an amplitude of 60%, sonication frequency of 20 kHz, and pulse intervals of 6 seconds on and 2 seconds off. After 1 hour of sonication, the ice bath was replaced. The suspensions were next centrifuged for 10 mins at 10,000 rpm. The yield was determined by drying 1 mL of suspension in an aluminum boat and weighing the final product after the water evaporated. To collect the exfoliated material, the suspension was vacuum filtered to remove the water and create a free-standing film. The films were then dried at 105°C, ground into fine powder, and vacuum dried at 105°C and 200°C separately for 24 hours. These samples are referred to as ex-LVO 105°C VD and ex-LVO 200°C VD, respectively.

Materials characterization

To obtain scanning electron microscopy (SEM) images of the nanoflakes, a dilute nanoflake suspension was drop cast onto an anodized alumina membrane (AAO; 0.02 µm pore size, Sterlitech) and vacuum filtered. This membrane was sputter-coated with a thin layer of Pt/Pd to prevent surface charge build up and improve image quality. The morphology of the nanoflakes

and free-standing films were captured using a Zeiss Supra 50VP SEM instrument equipped with a Schottky field emission and Everhart-Thornley in-lens secondary electron detectors using accelerating voltages of 5 kV and 3 kV, respectively. The phase composition of each material was analyzed using X-ray diffraction (XRD) with a SmartLab Rigaku X-ray diffractometer with Cu $K\alpha$ ($\lambda = 1.54$ Å) radiation and a step size of 0.02°. The d-spacing was calculated from the position of the (001) reflection using Bragg's law equation. Thermogravimetric analysis (TGA) was performed in air using a TA instruments Q50 instrument in a temperature range of 25°C to 1000°C and heat ramp of 10°C min⁻¹ under ambient conditions. To gather further structural information related to V-O bonding, Raman spectra were collected from 100 to 2500 cm⁻¹ using a Renishaw inVia Raman microscope (Renishaw, United Kingdom) with 514 nm Ar-ion laser. X-ray photoelectron spectroscopy (XPS) measurements were recorded on a Physical Electronics VersaProbe 5000 using a monochromatic Al Kα source and charge compensation. The highresolution V 2p spectra were taken at a pass energy of 23.5 eV with a step size of 0.05 eV. Peak fitting and data analysis were carried out using CasaXPS software. A Shirley background was used for V 2p spectra quantification. For the scanning transmission electron microscopy (STEM) analysis, the samples were dried at 105°C and 200°C in a form of the free-standing films obtained via vacuum filtration of the exfoliated nanoflakes without grinding. Cross-sectional STEM samples were prepared from these films by standard focused ion beam (FIB) techniques. STEM experiments were performed on a Nion UltraSTEM 100 operated at 100 keV with a convergence semiangle of ~31 mrad and a beam current of ~35 pA. Bright-field (BF)-STEM images were acquired up to a maximum semiangle of \sim 7 mrad and with a dose of \sim 3 x 10³ e⁻/Å², which is less than the damage threshold for the material, determined to be $\sim 10^4$ e⁻/Å² by tracking loss of atomicscale structure in image series. Local layer orientation mapping was performed by taking a series of fast Fourier transforms (FFTs) in small windows across the BF-STEM images, identifying the angle and intensity of the FFT peaks arising from the material lattice in the each, and visualizing them in a quiver plot with additional background color/intensity. All data was processed in Python using standard packages. Samples were stored in a vacuum desiccator, other than during FIB preparation and STEM experiments.

Electrode Fabrication

The electrodes were prepared by combining the dried LVO active material, acetylene carbon black, and PVDF binder with NMP solvent in a weight ratio of 70:20:10. The slurry was prepared by wet mixing and grinding the components using a mortar and pestle with the addition of NMP solvent. The slurry was then cast onto an Al foil current collector and dried in a vacuum oven at 120°C overnight. The dried electrode film was punched into 10 mm disks and vacuum dried at 105°C overnight prior to cell assembly. Coin cells were assembled in an argon filled glovebox.

Electrochemical Testing

The electrochemical cells were assembled using a half cell CR 2032 type coin cell configuration. Cell components consisted of lithium metal foil (Alfa Aesar) as the counter and reference electrodes, LVO as the working electrode, polypropylene membrane (2325, Celgard USA) as the separator, and commercial LP40 (Gotion, 1M LiPF₆ in 1:1 vol/vol ethylene carbonate (EC)/ diethyl carbonate (DEC)) as the electrolyte. All electrochemical tests were performed in a voltage rage of 2.0 – 4.0 V vs. Li/Li⁺. Cyclic voltammetry measurements were performed using a BioLogic VP3 potentiostat, and the cells were cycled at a sweep rate of 0.1 mV s⁻¹. Galvanostatic charge and discharge cycling was conducted at a specific current of 20 mA g⁻¹. The rate capability experiments were performed by cycling cells for 10 cycles at specific currents of 20, 50, 100, 200 mA g⁻¹, and 20 mA g⁻¹. Both cycling stability and rate capability tests were performed using an Arbin battery testing station. All potentials are reported with respect to the Li/Li⁺ reference electrode.

3. Results and Discussion

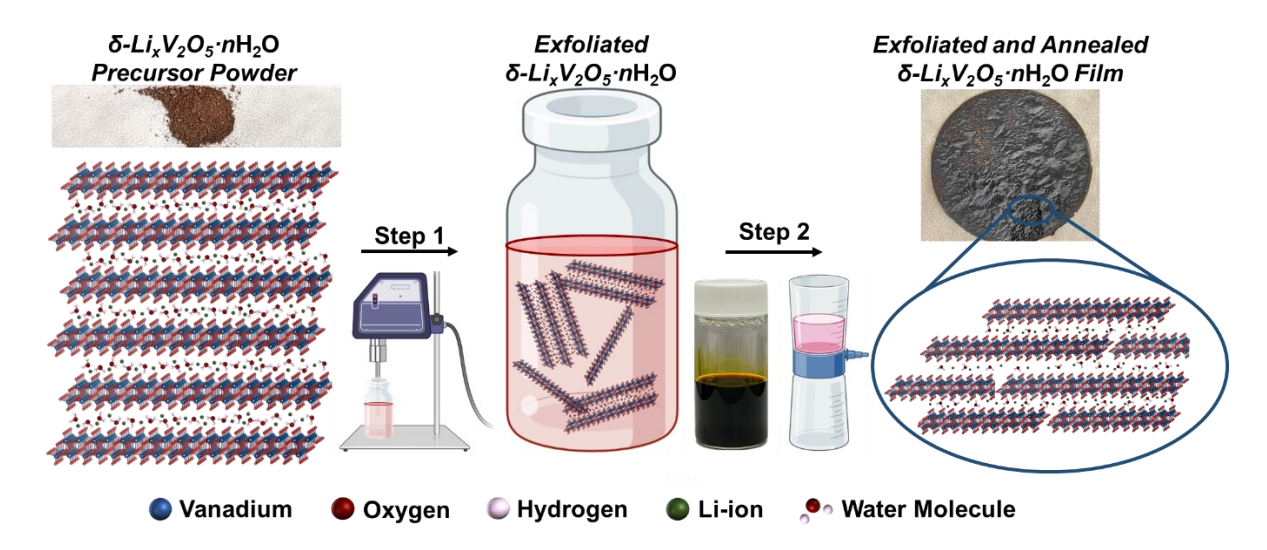


Figure 1. Schematic illustration of sonication (Step 1) and vacuum filtration (Step 2) processes used to produce exfoliated δ -Li_xV₂O₅·nH₂O (LVO) nanoflakes and free-standing films. Photographs of the precursor powder and free-standing film are shown next to the corresponding structure schematics. Created with BioRender.com.

The exfoliation, filtration, and drying processes used to produce free-standing LVO films are outlined in **Figure 1**. After sonication and centrifugation, a dark liquid containing LVO particles was collected without evident agglomeration as suggested by a relatively high magnitude zeta potential value of -31.4 (**Figure S1** in **Supporting Information**). The liquid was characterized as a colloidal suspension containing exfoliated LVO particles through the observation of a Tyndall scattering effect. **Figure 2a** shows that a laser light shone through the side of a glass vial across the diluted liquid formed a visible line, indicating that the dispersed LVO particles did not dissolve from the sonication process and led to the scattering of laser light. Gravimetric measurements were performed to calculate the concentration of the exfoliated and centrifuged LVO. The initial suspension prior to exfoliation and centrifugation had a concentration of 10 mg·mL⁻¹, and multiple measurements found a final average concentration of 9.71 mg·mL⁻¹. This result suggests that the LPE of LVO in aqueous media facilitates a high yield, in contrast to other suggested compatible organic solvents based on optimal solubility parameters.²¹

SEM imaging was performed to identify the morphology of the exfoliated LVO particles. The SEM image shown in **Figure 2b** is a single LVO nanoflake obtained after exfoliation that has a flat flake-like shape. Compared to the SEM image of bulk LVO precursor particles obtained by

Information), the exfoliated LVO nanoflake has a 2D shape, and it is smaller in size than the particles of the precursor powder which have clumped into an irregularly shaped morphology. The differences in morphology and size of the particles show the different results achieved by mechanical shearing via probe tip compared to shear from stirring induced turbulence. This difference indicates that the probe tip generates enough sonication energy to straighten the bulk precursor particles and delaminate them into flakes. Although the mechanism of exfoliation is beyond the scope of this work, it is believed that water molecules could also play a role in the reduction of flake size and forces between the layers due to the affinity of vanadium oxides for water molecules and partial dissolution.

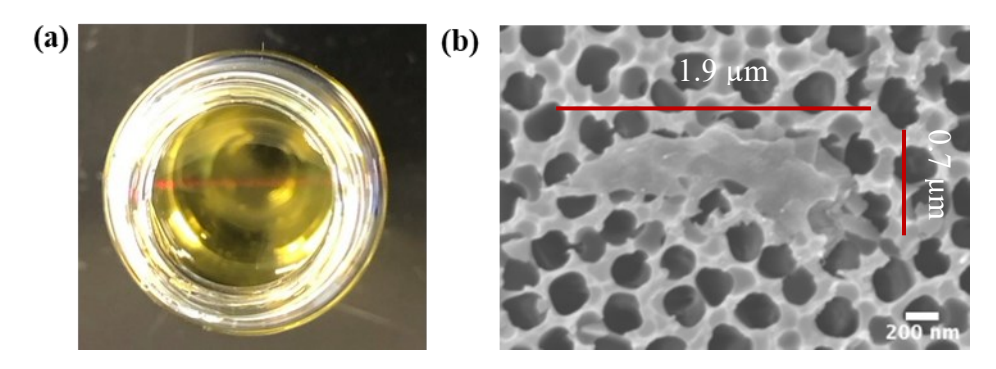


Figure 2. (a) Tyndall scattering experiment performed on a dilute exfoliated LVO suspension with a visible red laser scattered by suspended particles (b) SEM image of the LVO nanoflake deposited on anodized alumina (AAO) membrane.

Of note, the use of water as a solvent during the exfoliation process could result in an excessive hydration of LVO nanoflakes where water is physiosorbed and structural water is introduced to the material. Studies have shown that the water content of bilayered vanadium oxide greatly affects its electrochemical performance in non-aqueous Li-ion cells. As a result, it is of interest to evaluate and establish drying protocols for controlling water content of LVO nanoflakes after exfoliation in aqueous media. To understand the effect of water as a solvent in the exfoliation process on charge storage properties, free-standing LVO nanoflake films were ground and vacuum dried at different temperatures. A previous study details the thermal analysis of hydrothermally treated δ -Na_xV₂O₅·nH₂O synthesized under similar conditions as LVO reported in this study. If It was proposed that vacuum annealing the material at 100° C enabled the removal of physically

adsorbed water and that 260°C was the maximum annealing temperature to remove structural water while preserving the bilayered structure. However, vacuum drying the ground LVO nanoflakes in this study at 250°C initiated the onset of structural change, which will be discussed later. Therefore, the drying temperatures selected for comparison were 105°C and 200°C.

Cross-sectional SEM images of the films dried at temperatures of 105°C and 200°C under vacuum are shown in **Figure 3**. Both images demonstrate a lamellar morphology consisting of stacked nanoflakes that are assembled into a film. The areas with tightly stacked nanoflakes alternate with the areas where the nanoflakes are more separated. The SEM image of ex-LVO 200°C VD film shows slightly more planar and ordered nanoflakes compared to the ex-LVO 105°C VD film. In comparison, the free-standing film obtained by vacuum filtration of the bilayered vanadium oxide exfoliated in NMP^[13] demonstrated a more pronounced curvature of the nanoflakes and large voids formed between the individual nanoflakes stacked into a film. Here, when using water as a medium for exfoliation, we observed predominantly flat nanoflakes assembled together in a dense stacked structure during vacuum filtration. The observed film architecture could be due to the interactions between the flakes caused by the water molecules absorbed onto the nanoflake surface during the aqueous exfoliation process.

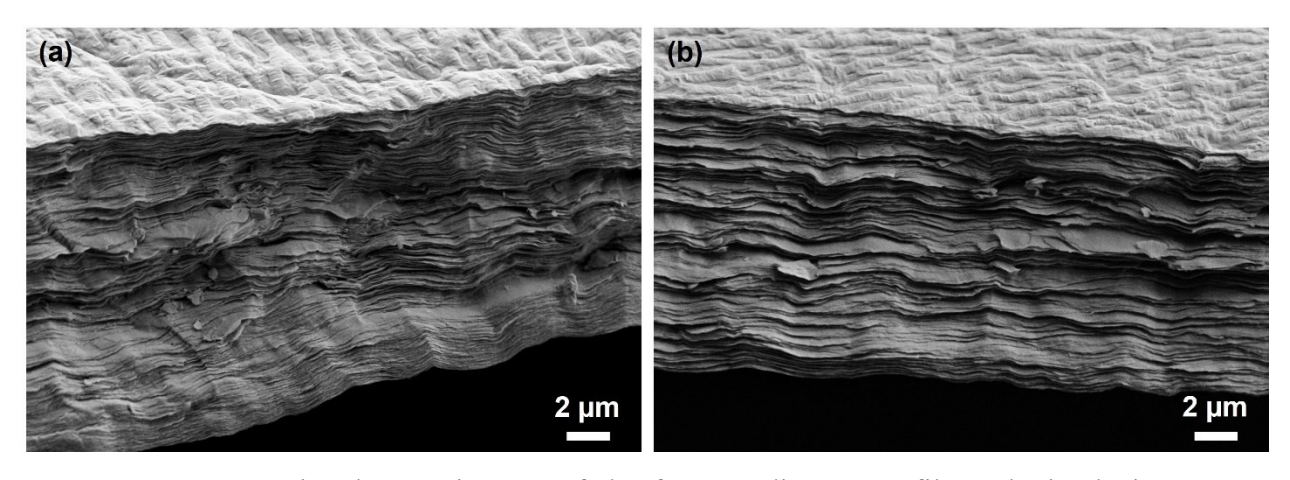


Figure 3. Cross sectional SEM images of the free-standing LVO films obtained via vacuum filtration of the exfoliated nanoflakes and drying under vacuum at (a) 105°C and (b) 200°C.

XRD patterns of the precursor powders and ground free-standing films obtained through the vacuum filtration of exfoliated LVO suspensions and dried at 105°C and 200°C under vacuum are shown in **Figure 4a**. The series of (00*l*) reflections in the XRD patterns of all samples are

characteristic of bilayered vanadium oxide,⁵ indicating that no structural transformations occurred as a result of exfoliation or drying process. In both the bulk LVO precursor and exfoliated LVO samples, there are apparent decreases in *d*-spacings from 12.246Å to 11.617Å and 12.117Å to 11.647Å, respectively, when the vacuum drying temperature is increased from 105°C to 200°C. Increasing drying temperatures to 250°C, however, resulted in the formation of VO_x impurities (**Figure S3** in **Supporting Information**), indicating the decomposition of the bilayered phase.

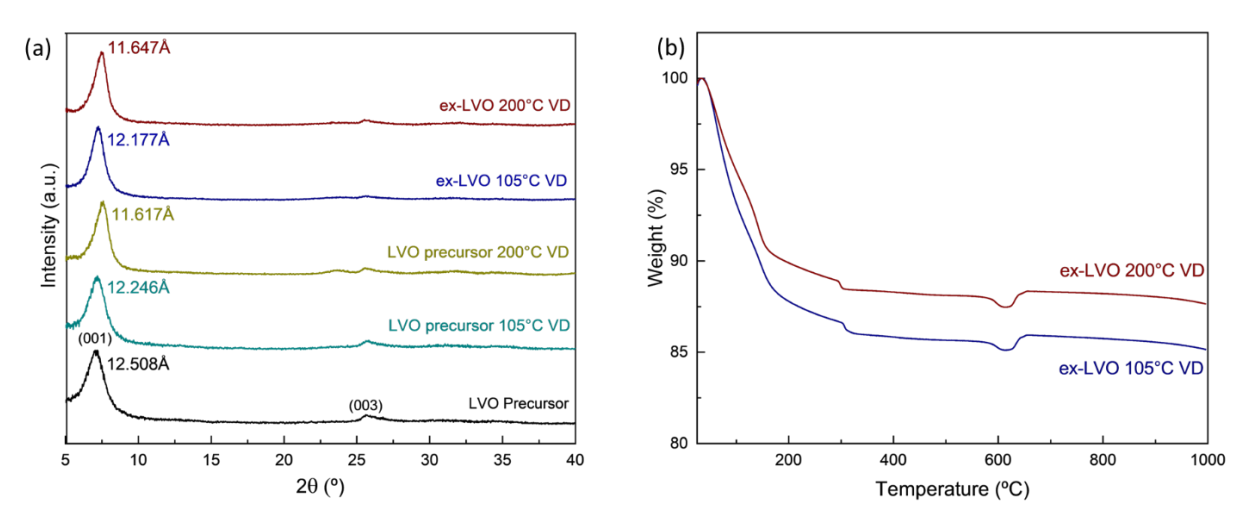


Figure 4. Phase composition and thermal analysis characterization of the LVO precursors and free-standing LVO films formed by vacuum filtration of the nanoflakes obtained by exfoliating the powder precursor in water. (a) XRD patterns of the vacuum dried samples and (b) TGA curve of the films dried at 105°C and 200°C.

LPE exfoliation in aqueous media can introduce loosely bound physiosorbed and crystallographic water in the interlayer region of LVO, both of which add to the complex mechanism of water removal. However, distinct temperature ranges can be associated with the removal of different species of water as demonstrated in the previous report. In summary, it was reported that the temperature region of 25-100°C corresponds to the removal of physically adsorbed water and 100-510°C corresponds to the removal of crystallographic water, first from the interlayer region of the bilayered vanadium oxide framework, and then from the structure of the heat induced transformation product. Therefore, in this study we used the weight loss in the temperature range of 100-510°C to evaluate the hydration degree of the ex-LVO samples dried at 105°C and 200°C under vacuum. TGA weight loss curves displayed in **Figure 4b** show 14.35% and 11.90% weight loss in the temperature range of 25-510°C for the free-standing LVO films

dried at 105°C and 200°C. This weight loss corresponds to the water molecules that could cause parasitic reactions during electrochemical cycling of the hydrated electrodes in non-aqueous energy storage systems. The free-standing LVO film vacuum dried at 105°C experienced 2.45% greater weight loss, which is ascribed to the removal of crystallographic water that requires higher temperatures and could not be removed by vacuum drying at 105°C. The TGA data analysis complements our observation with the XRD patterns, where the samples vacuum dried at 105°C have larger interlayer spacings due to the higher hydration degree.

To explore the nano- and atomic-scale structure of the flakes, aberration-corrected BF-STEM imaging was performed, as shown in Figure 5. In these images, the flakes are oriented with the [001] direction facing up, as in Figure 3, and the vanadium oxide bilayer and interlayer spacing regions give rise to the periodic bright and dark lines observed. Films dried at 105°C and 200°C both exhibited layered atomic structures that were generally oriented in a consistent direction, with the 200°C film having a more homogeneous set of local orientations of the layers, as shown in the quiver plots of Figures 5b and 5e. The 200°C film in particular had a nearly continuous atomic lattice structure across many microns, as shown in Figure S4 (Supporting Information), indicating that the flakes were well-bonded to each other. In addition to the layered structure, a single-crystal region that contained nanoscale voids was also observed in the 105°C sample, as shown in Figure S5 (Supporting Information), but understanding this structure will require a separate study. From the STEM measurements, interlayer spacings of the materials could be measured as well, with the results shown in Figures 5c and 5f. From these measurements, the interlayer spacings were 8.3 ± 0.7 Å and 9.1 ± 0.4 Å for the films dried at 105° C and 200° C, respectively. Similarly to the bilayered vanadium oxide films obtained by the vacuum filtration of the nanoflakes exfoliated in NMP^[13], the discrepancy between the interlayer spacings measured through XRD and STEM could be related to the bulk and local nature of the measurements, respectively, as well as the film processing conditions required for the preparation of the sample for imaging. Overall, the structure of the films was well-ordered at the nanometer scale and highly crystalline at the atomic scale, especially for the film dried at 200°C.

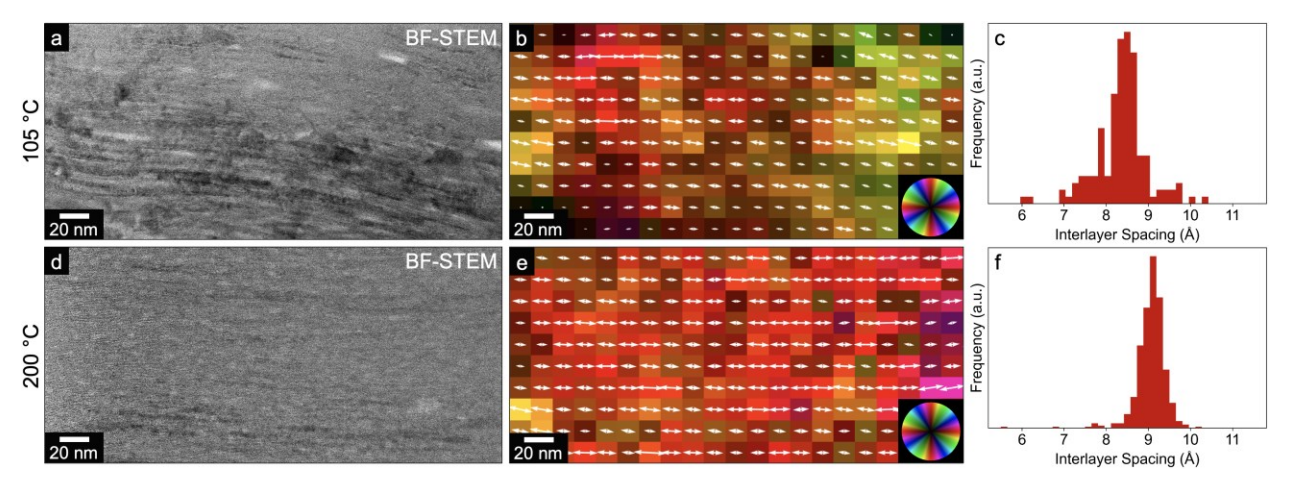
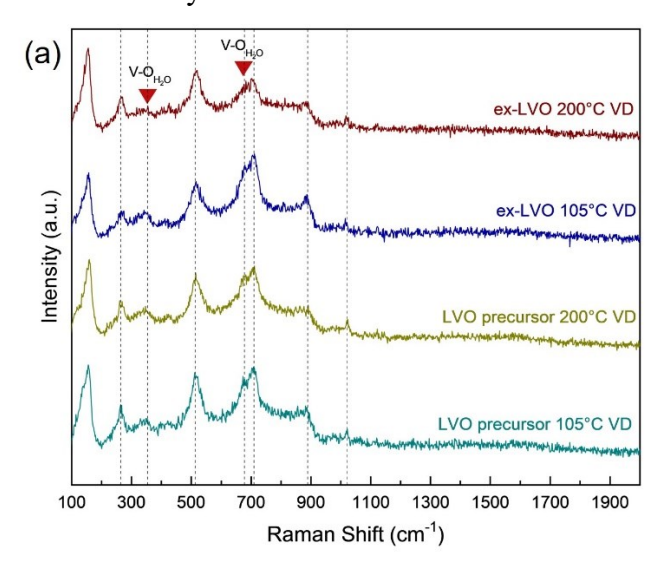


Figure 5. Cross sectional (a) BF-STEM image and corresponding local (b) lattice orientation and (c) interlayer spacing information from approximately the same region of an LVO film obtained via vacuum filtration of exfoliated nanoflakes and drying under vacuum at 105°C. (d-f) Same as (a-c), but for a film vacuum dried at 200°C. Arrow lengths and directions in (b) and (e), as well as background brightness and color, are proportional to local lattice contrast and orientation, respectively. Average arrow lengths/background brightnesses are normalized from left to right in (e) to compensate for slowly changing contrast due to thickness variation.

LPE via probe tip sonication produces enough energy to form defects in the LVO layers after exfoliation. 12 In order to quantify the extent of defect formation and monitor the relative concentration of water between drying steps, Raman spectroscopy was used to measure the types of vibrational modes present in the precursor and exfoliated materials. The Raman spectra of LVO powders and free-standing films are given in Figure 6a. Common prominent peaks are denoted by dotted lines; each of these peaks are assigned using the descriptions given in **Table 1**, while the specific atoms are shown in the structure schematic shown in Figure 6b. V₁ and V₂ are the intralayer vanadium atoms occupying different crystallographic positions. This distinction arises from the difference in bond lengths between V₁-O₂ and V₂-O₃^[16]. O₁ refers to a triply coordinated oxygen atom sitting between in-plane vanadium atoms, O₂ is a quadruple coordinated oxygen outof-plane bonded to V₁, O₃ is a quadruple coordinated oxygen out-of-plane bonded to V₃, O₄ is a terminal oxygen bonded to V₁, O₅ is a terminal oxygen bonded to V₂. O_{water} refers to the oxygen found in the interlayer water molecules. Raman spectra for the precursor and exfoliated materials are in good agreement with previously reported bilayered vanadium oxides.²² All samples contained similar features, only with differences in attenuation. The features identified up to ~1000 cm⁻¹ constitute the fingerprint region of the δ-V₂O₅ phase. Two features, the V-O_{water} bending at ~350 cm⁻¹ and the V-O_{water} stretching at ~675 cm⁻¹ features correspond to the interactions of the interlayer water with the vanadium atoms in each layer of the bilayered structure. While both precursor materials show no difference in intensities of these features, in the exfoliated materials the intensities are significantly reduced in the 200°C-dried sample compared to the 105°C-dried sample, indicating the reduction in interlayer water content for exfoliated LVO vacuum dried at 200°C. This observation is in agreement with the reduced d-spacing and lower hydration degree indicated by the XRD and TGA data analysis.



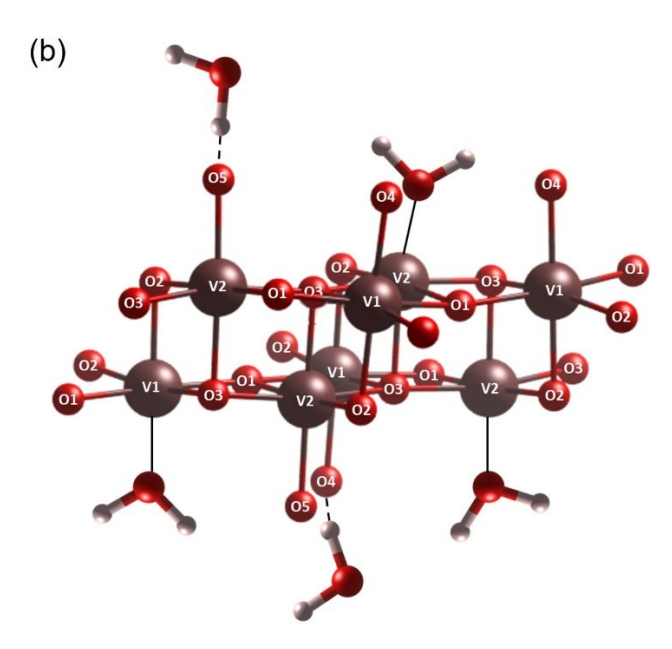


Figure 6. (a) Raman spectra of δ -Li_xV₂O₅·*n*H₂O precursor powder and ground δ -Li_xV₂O₅·*n*H₂O free-standing films obtained by the vacuum filtration of the exfoliated nanoflakes that were vacuum dried at 105°C and 200°C, and (b) schematic illustration of V-O bilayer structure showing interactions with the interlayer water molecules.

Table 1. Peak assignments of Raman spectra of δ-Li_xV₂O₅·*n*H₂O materials shown in Figure 6a in comparison with literature data. O_{water} refers to the oxygen found in the surrounding water molecules.

Material	Skeletal bending	$V_1 - O_2 - V_2$ bending	V _(1,2) – O _{water} bending	V ₁ - O ₄ bending	$V_{(1,2)} - O_{water}$ stretching	V _(1,2) – O ₂ stretching	Intralayer $V_1 - O_3 - V_2$ bending	V ₂ = O ₅ stretchin g
$\begin{array}{c} \delta\text{-} \\ \text{Na}_{x}\text{V}_{2}\text{O}_{5}\text{\cdot}\text{nH}_{2}\text{O}^{[16]} \end{array}$	153	288	N/A	508	N/A	702	878	1007
δ- $\text{Li}_{x}\text{V}_{2}\text{O}_{5}\cdot\text{nH}_{2}\text{O}^{[23]}$	157	265	N/A	519	N/A	702	N/A	1021
This work	156	265	350	516	675	703	886	1018

Analysis of the V_{2p} XPS spectra shown in Figure 6a revealed that vanadium exists in a mixed pentavalent (V⁵⁺) and tetravalent (V⁴⁺) oxidation states in both precursor materials. This partial reduction of vanadium occurs due to the introduction of chemically pre-intercalated Li⁺ ions into the interlayer region during the sol-gel synthesis of the bulk precursor material. The precursors dried at 105 °C and 200 °C have average vanadium oxidation states of +4.8 and +4.75, respectively. Drying the precursor at 200 °C likely induced additional vanadium reduction from the formation of oxygen vacancies, a phenomenon observed in a previous study that reported reduced vanadium in V₂O₅ aerogels and ambigels heated under vacuum at a temperature of 220 °C using X-ray absorption spectroscopy.²⁴ Of note, the exfoliated materials dried at 105 °C and 200 °C have an approximate average vanadium oxidation state of +5.0 and +4.9, respectively. A previous study also observed the reduction of vanadium in V₂O₅ thin films treated at 200 °C under ultra-high vacuum, again explained by the formation of oxygen vacancies. ²⁵ The XPS data analysis is summarized in Table 2. The higher average oxidation state of the free-standing films compared to the powder could be explained by both the removal of Li⁺ ions from the interlayer spacing during exfoliation as well as the exposure of LVO to the oxidizing aqueous environment during exfoliation, which contrasts to our previous work with exfoliation done in NMP.¹³

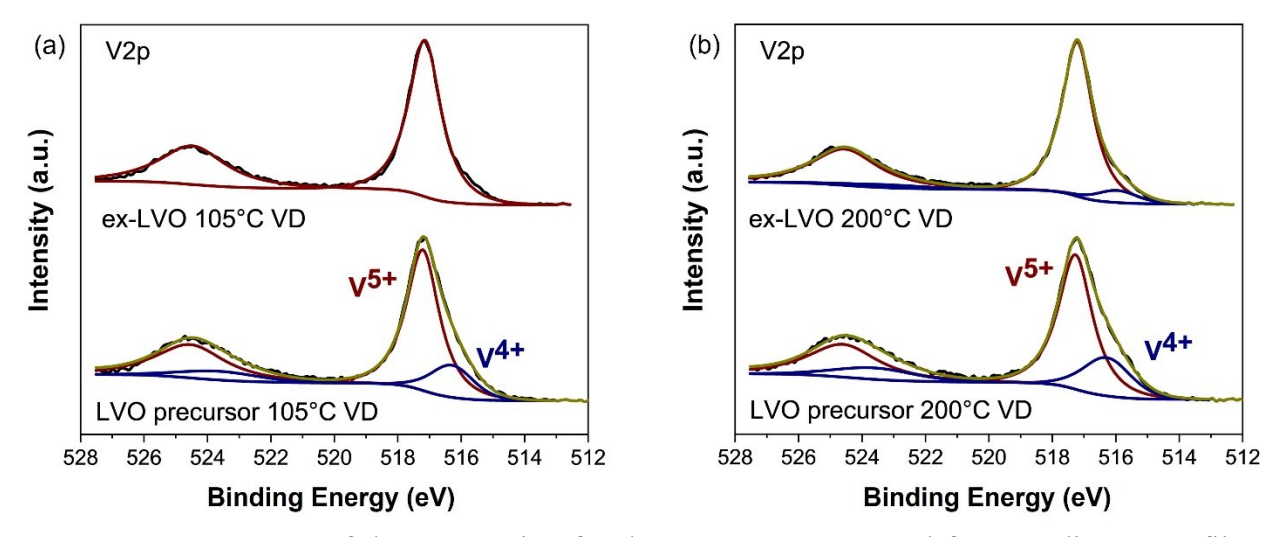


Figure 7. XPS spectra of the V2p region for the LVO precursors and free-standing LVO films formed by vacuum filtration of the nanoflakes obtained by exfoliating the powder precursor in water dried at (a) 105 °C and (b) 200 °C.

Table 2. Summary table of XPS data analysis reporting fractions of V^{5+} and V^{4+} atoms in the precursor and exfoliated materials

Sample	V ⁵⁺ Atomic %	V ⁴⁺ Atomic %		
precursor LVO 105°C VD	80	20		
precursor LVO 200°C VD	74	26		
ex-LVO 105°C VD	100	0		
ex-LVO 200°C VD	92	8		

To assess the capabilities of the LVO nanoflakes as a cathode material for Li⁺ ion storage and study the effects of vacuum drying temperature on their electrochemical performance, LVO nanoflake electrodes were tested in Li-ion half coin cells. The electrochemical performance of the LVO nanoflakes dried at 105°C and 200°C are shown in **Figure 8**. Cyclic voltammetry was performed to evaluate the charge storage processes for ex-LVO 105°C VD and ex-LVO 200°C VD. Shown in **Figure 8a** and **8b**, both materials dried at different temperatures demonstrate cathodic peaks at 2.43 V and 2.80 V and anodic peaks at 2.64 V and 3.00 V. Furthermore, a potential difference between cathodic and anodic peaks of ~200mV indicates high reversibility of intercalation/deintercalation process. The shape of the CV curves is similar to other previously reported hydrated vanadium pentoxides synthesized via sol-gel method. This suggests that the exfoliation process and change in morphology of our nanoflake material does not alter the charge storage process of the bilayered vanadium oxide. The specific currents in CV curves of the cell containing ex-LVO 200°C VD electrode are higher compared to the cell with the ex-LVO 105°C

VD electrode, indicating improved ion intercalation achieved after vacuum drying at higher temperature. This improvement can be attributed to the removal of excess water from the interlayer region when drying at elevated temperatures.

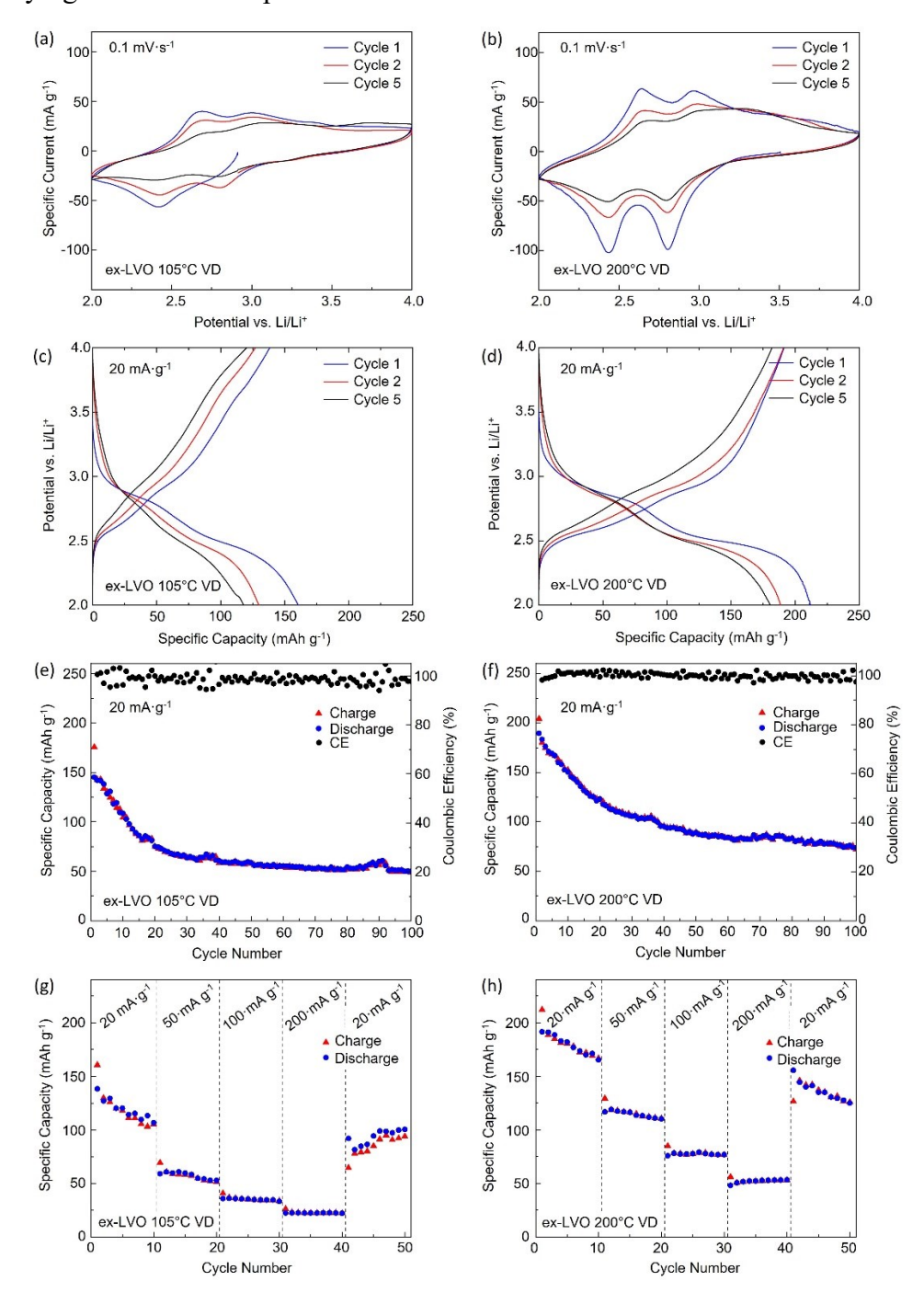


Figure 8. Electrochemical testing of the films composed of exfoliated LVO nanoflakes dried at (a,c,e,g) 105°C and (b,d,f,h) 200°C; (a,b) 1st, 2nd and 5th cycle CV curves at a sweep rate of 0.1 mV·s⁻¹, (c,d) 1st, 2nd and 5th cycle galvanostatic charge/discharge curves and (g, f) cycle life testing for 100 cycles at a current density of 20 mA·g⁻¹, and (e,f) rate capability testing at current densities of 20, 50, 100, and 200 mA·g⁻¹ in 10 cycle intervals.

The galvanostatic discharge/charge curves of the first, second, and fifth Li⁺ ion insertion/extraction cycles of exfoliated LVO 105°C VD and LVO 200°C VD at a current density of 20 mA·g⁻¹ are displayed in **Figure 8c** and **8d**. The initial specific discharge capacity of LVO 200°C VD (212 mAh·g⁻¹) exceeds that of LVO 105°C VD (160.6 mAh·g⁻¹) which is in agreement with the CV data. This decreased capacity for LVO 105°C VD could be attributed to more water occupying redox active sites which inhibits the intercalation and storage of Li⁺. This phenomenon has been reported in the case of vanadium oxide gels with sodium ions.¹⁷ Furthermore, the sample dried at 105°C experiences a much greater capacity fade with ~30% capacity retention by the fifth cycle which suggests poorer cycling stability as a result of the increased water content.

To further understand how water content affects the cycling stability of exfoliated LVO, galvanostatic cycling was performed at a current density of 20 mA·g⁻¹ for 100 cycles for ex-LVO 105°C and 200°C VD cathodes (Figure 8e, 8f). After 100 cycles, the ex-LVO 105°C electrode delivered a specific discharge capacity of 49.02 mAh·g⁻¹ with a capacity retention of 27.9%. The ex-LVO 200°C VD electrode demonstrated a higher specific discharge capacity of 64.7 mAh·g⁻¹ and higher retention of 35.3%; this behavior is in agreement with the improvements observed in cyclic voltammetry experiments. Despite the lowered water content illustrated by the TGA, the ex-LVO 200°C VD still contains water that contributes to parasitic processes that hamper capacity fade and cycling stability. There are several mechanisms of capacity fade that can be caused by structural water. One is the hydrolysis of lithium hexafluorophosphate (LiPF₆), which is an essential ingredient in commercial electrolytes, and is used in this study. ²⁶ This generates HF gas, and has been noted to cause dissolution of V₂O₅ in previous reports.²⁷ Another possible mechanism for capacity fade is the reaction between Li ions and structural water leading to the formation of inactive LiOH species. This has previously been observed for V₂O₅ aerogels containing tightly bound water.²⁸ It has been proposed that capacity fade for the bilayered phase of vanadium oxide could also be attributed to electrode pulverization of the cathode during cycling or formation of irreversible phases.²⁹ Further post mortem analysis would need to be conducted to comprehensively diagnose the processes affecting electrochemical behavior of the free-standing LVO films and develop strategies for improvements.

Rate capability experiments were performed to assess the tolerance of ex-LVO 105°C VD and ex-LVO 200°C VD cathodes to increasingly high specific currents at 10 cycle intervals (**Figure 8g, 8h**). An average specific discharge capacity is calculated for each 10 cycle interval to

compare capacity and capacity retentions at different current densities. The average discharge capacity for ex-LVO 105°C VD and ex-LVO 200°C VD over 10 cycles at the initial current density of 20 mA·g⁻¹ are 119.04 and 180.53 mAh·g⁻¹, respectively. After increasing the current density to 200 mAh·g⁻¹, the discharge capacities are 23.11 and 52.61 mAh·g⁻¹, respectively; this corresponds to a capacity retention of 19.41% and 29.14% and shows that ex-LVO 200°C VD maintains higher capacities at higher current densities. After returning the current density back to 20 mA·g⁻¹ from 200 mA·g⁻¹ (cycles 41-50), the average capacity for ex-LVO 105°C VD and ex-LVO 200°C VD is 85.08 mAh·g⁻¹ (capacity retention of 71.5%) and 135.38 mAh·g⁻¹ (capacity retention of 74.4%), respectively. Based on these values, there is no significant difference between ex-LVO 105°C VD and ex-LVO 200°C VD's ability to tolerate high current densities. Still, the absolute capacity value obtained in the rate capability experiment at 200 mA·g⁻¹ is higher in case of the ex-LVO 200°C VD electrode, which could be attributed to a larger number of intercalation sites available due to the more efficient removal of the interlayer water compared to the material dried at 105°C. These results suggest that while increased water content does decrease ion storage capacity and decrease capacity retention at higher current densities, it does not greatly affect LVO's tolerance to high currents after cycling through increasing current densities. Interestingly, the discharge capacities for ex-LVO 105°C VD and ex-LVO 200°C VD (94.03 and 124.96 mAh·g⁻¹) at cycle 50 in rate capability tests were greater than what was observed from the life cycle tests (57.99 and 80.25 mAh·g⁻¹) at a consistent low current density of 20 mA·g⁻¹. It is believed that this could be related to the progressing formation of LiOH, which is likely more prevalent when the ex-LVO cathodes are cycled repeatedly at lower current densities.

4. Conclusion

In this work, we have demonstrated a simple liquid phase exfoliation technique for the exfoliation of bulk δ -Li_xV₂O₅·nH₂O (LVO) in water. Probe tip sonication of the material was applied to acquire a colloidal suspension of LVO with high yield after centrifugation. Water is safer, more cost effective, and produces a higher yield relative to exfoliation in NMP solvent performed in previous work. Imaging revealed a flat nanoflake like morphology of the exfoliated particles. Using vacuum filtration to remove the solvent, the flakes assembled into a thin and flexible free-standing film with an ordered lamellar structure. XRD showed that the exfoliation process on the bulk particles did not induce any structural transformation. This work further

explores the use of vacuum drying to control the interlayer water content present in exfoliated LVO as a result of exposure to an aqueous environment during exfoliation. Vacuum drying was conducted at 105°C and 200°C on ground LVO films (ex-LVO 105°C and ex-LVO 200°C VD). XRD patterns revealed a decrease in interlayer spacing from 12.18Å to 11.65Å due to the reduction of interlayer water content accompanying an increase in vacuum drying temperature form 105°C to 200°C. TGA showed that ex-LVO 105°C VD experienced a 2.08% greater weight loss than ex-LVO 200°C VD between 25-200°C, which is attributed to the 105°C dried sample containing more structural water. Furthermore, the Raman spectra of ex-LVO 200°C VD showed decreased peak intensities at 350 and 675 cm⁻¹ that correspond to V-OH stretching modes, which indicates less structural water present in the sample following a higher drying temperature. Electrochemical testing of the Li-ion half coin cells containing the ex-LVO 105°C VD and ex-LVO 200°C VD electrodes revealed that the elevated drying temperature led to increased specific capacities, which is likely to be associated with the lower interlayer water content. Extended cycling results demonstrated that the ex-LVO 200°C VD electrodes have a 7.4% greater capacity retention than the material dried at 105°C after 100 cycles. However, low capacity retention of 35.3% suggest that retained interlayer water in the material could still induce capacity fading. Overall, these results demonstrate the importance of controlling interlayer water content of hydrated LVO for improving ion storage capacity and electrochemical stability. The exfoliation of LVO in water producing nanoflakes with high yield has opened pathways towards their integration with other 2D nanomaterials using liquid-based assembly methods to fabricate 2D heterostructures for energy storage applications.

Supporting Information contains zeta potential curve of δ -Li_xV₂O₅·nH₂O nanoflakes dispersed in water obtained after exfoliation, SEM image of δ -Li_xV₂O₅·nH₂O precursor powder, XRD patterns of pristine δ -Li_xV₂O₅·nH₂O nanoflake film and the one dried at 250°C, overall structure of the FIB-prepared dried films, imaged with a highly defocused STEM probe, and BF-STEM image of a single-crystal region of the film dried at 105°C and the corresponding fast Fourier transform with lattice spacings.

Acknowledgements

This work was supported by the National Science Foundation (NSF) under Grant No. DMR-1752623. We acknowledge Drexel's Materials Characterization Core (MCC) facility for providing access to characterization instruments. The scanning transmission electron microscopy portion of this research was supported by the Center for Nanophase Materials Sciences (CNMS), which is a US Department of Energy, Office of Science User Facility at Oak Ridge National Laboratory.

References

- (1) (a) Cui, H.; Guo, Y.; Ma, W.; Zhou, Z. 2 D materials for electrochemical energy storage: design, preparation, and application. *ChemSusChem* **2020**, *13* (6), 1155-1171. (b) Xu, B.; Qi, S.; Jin, M.; Cai, X.; Lai, L.; Sun, Z.; Han, X.; Lin, Z.; Shao, H.; Peng, P. 2020 roadmap on two-dimensional materials for energy storage and conversion. *Chinese Chemical Letters* **2019**, *30* (12), 2053-2064. (c) Liu, H.-J.; Dong, B. Recent advances and prospects of MXene-based materials for electrocatalysis and energy storage. *Materials Today Physics* **2021**, *20*, 100469. (d) Upadhyay, S. N.; Satrughna, J. A. K.; Pakhira, S. Recent advancements of two-dimensional transition metal dichalcogenides and their applications in electrocatalysis and energy storage. *Emergent Materials* **2021**, *4* (4), 951-970.
- (2) Pomerantseva, E. Chemical preintercalation synthesis of versatile electrode materials for electrochemical energy storage. *Accounts of Chemical Research* **2023** (accepted), DOI: 10.1021/acs.accounts.2c00193
- (3) Pomerantseva, E.; Gogotsi, Y. Two-dimensional heterostructures for energy storage. *Nature Energy* **2017**, *2*, 17089. DOI: http://dx.doi.org/10.1038/nenergy.2017.89 Engineering Collection; ProQuest One Academic.
- (4) Clites, M.; Pomerantseva, E. Bilayered vanadium oxides by chemical pre-intercalation of alkali and alkali-earth ions as battery electrodes. *Energy Storage Materials* **2018**, *11*, 30-37. DOI: https://doi.org/10.1016/j.ensm.2017.09.005.
- (5) Petkov, V.; Trikalitis, P. N.; Bozin, E. S.; Billinge, S. J. L.; Vogt, T.; Kanatzidis, M. G. Structure of V₂O₅·*n*H₂O Xerogel Solved by the Atomic Pair Distribution Function Technique. *Journal of the American Chemical Society* **2002**, *124* (34), 10157-10162. DOI: 10.1021/ja026143y. (6) Huang, X.; Qi, X.; Boey, F.; Zhang, H. Graphene-based composites. *Chemical Society Reviews* **2012**, *41* (2), 666-686.
- (7) (a) Clites, M.; Andris, R.; Cullen, D. A.; More, K. L.; Pomerantseva, E. Improving Electronic Conductivity of Layered Oxides through the Formation of Two-Dimensional Heterointerface for Intercalation Batteries. ACS Applied Energy Materials 2020, 3 (4), 3835-3844. (b) Liu, Q.; Li, Z.-F.; Liu, Y.; Zhang, H.; Ren, Y.; Sun, C.-J.; Lu, W.; Zhou, Y.; Stanciu, L.; Stach, E. A. Graphenemodified nanostructured vanadium pentoxide hybrids with extraordinary electrochemical performance for Li-ion batteries. *Nature communications* **2015**, 6 (1), 1-10. (c) Averianov, T.; Pomerantseva, E. Composite Li-ion battery cathodes formed via integration of carbon nanotubes or graphene nanoplatelets into chemical preintercalation synthesis of bilayered vanadium oxides. Journal of Alloys and Compounds 2022, 903, 163929. DOI: https://doi.org/10.1016/j.jallcom.2022.163929.
- (8) Xiong, P.; Ma, R.; Sakai, N.; Sasaki, T. Genuine unilamellar metal oxide nanosheets confined in a superlattice-like structure for superior energy storage. *ACS nano* **2018**, *12* (2), 1768-1777.
- (9) Xu, S.; Dall'Agnese, Y.; Li, J.; Gogotsi, Y.; Han, W. Thermally Reduced Graphene/MXene Film for Enhanced Li-ion Storage. *Chemistry–A European Journal* **2018**, *24* (69), 18556-18563.
- (10) Xiong, P.; Zhang, X.; Zhang, F.; Yi, D.; Zhang, J.; Sun, B.; Tian, H.; Shanmukaraj, D.; Rojo, T.; Armand, M. Two-dimensional unilamellar cation-deficient metal oxide nanosheet superlattices for high-rate sodium ion energy storage. *ACS nano* **2018**, *12* (12), 12337-12346.

- (11) Cai, X.; Luo, Y.; Liu, B.; Cheng, H.-M. Preparation of 2D material dispersions and their applications. *Chemical Society Reviews* **2018**, *47* (16), 6224-6266, 10.1039/C8CS00254A. DOI: 10.1039/C8CS00254A.
- (12) Backes, C.; Higgins, T. M.; Kelly, A.; Boland, C.; Harvey, A.; Hanlon, D.; Coleman, J. N. Guidelines for Exfoliation, Characterization and Processing of Layered Materials Produced by Liquid Exfoliation. *Chemistry of Materials* **2017**, *29* (1), 243-255. DOI: 10.1021/acs.chemmater.6b03335.
- (13) Houseman, L.; Mukherjee, S.; Andris, R.; Zachman, M. J.; Pomerantseva, E. Free-standing bilayered vanadium oxide films synthesized by liquid exfoliation of chemically preintercalated δ-Li_xV₂O₅·nH₂O. *Materials Advances* **2021**, *2* (8), 2711-2718. DOI: 10.1039/d1ma00085c.
- (14) Hunt, A.; Dale, N. Economic valuation in 1-Methyl-2-pyrrolidone (NMP) regulation. 2018.
- (15) (a) Maleski, K.; Mochalin, V. N.; Gogotsi, Y. Dispersions of Two-Dimensional Titanium Carbide MXene in Organic Solvents. *Chemistry of Materials* **2017**, *29* (4), 1632-1640. DOI: 10.1021/acs.chemmater.6b04830. (b) Compton, O. C.; Nguyen, S. T. Graphene oxide, highly reduced graphene oxide, and graphene: versatile building blocks for carbon-based materials. *small* **2010**, *6* (6), 711-723. Lee, H.; Dellatore, S. M.; Miller, W. M.; Messersmith, P. B. Mussel-inspired surface chemistry for multifunctional coatings. *science* **2007**, *318* (5849), 426-430.
- (16) Clites, M.; Hart, J. L.; Taheri, M. L.; Pomerantseva, E. Annealing-Assisted Enhancement of Electrochemical Stability of Na-Preintercalated Bilayered Vanadium Oxide Electrodes in Na-Ion Batteries. *ACS Applied Energy Materials* **2020**, *3* (1), 1063-1075. DOI: 10.1021/acsaem.9b02098.
- (17) Lee, C.-Y.; Marschilok, A. C.; Subramanian, A.; Takeuchi, K. J.; Takeuchi, E. S. Synthesis and characterization of sodium vanadium oxide gels: the effects of water (n) and sodium (x) content on the electrochemistry of Na_xV₂O₅·nH₂O. **2011**, 13 (40), 18047. DOI: 10.1039/c1cp21658a.
- (18) Wang, J.; Curtis, C. J.; Schulz, D. L.; Zhang, J.-G. Influences of Treatment Temperature and Water Content on Capacity and Rechargeability of V₂O₅ Xerogel Films. *Journal of The Electrochemical Society* **2004**, *151* (1), A1. DOI: 10.1149/1.1627342.
- (19) (a) Frey, N. C.; Byles, B. W.; Kumar, H.; Er, D.; Pomerantseva, E.; Shenoy, V. B. Prediction of optimal structural water concentration for maximized performance in tunnel manganese oxide electrodes. *Physical Chemistry Chemical Physics* **2018**, *20* (14), 9480-9487. DOI: 10.1039/c8cp00761f. (b) Wangoh, L. W.; Huang, Y.; Jezorek, R. L.; Kehoe, A. B.; Watson, G. W.; Omenya, F.; Quackenbush, N. F.; Chernova, N. A.; Whittingham, M. S.; Piper, L. F. Correlating lithium hydroxyl accumulation with capacity retention in V₂O₅ aerogel cathodes. *ACS applied materials & interfaces* **2016**, *8* (18), 11532-11538.
- (20) (a) Geng, Y.; Pan, L.; Peng, Z.; Sun, Z.; Lin, H.; Mao, C.; Wang, L.; Dai, L.; Liu, H.; Pan, K.; et al. Electrolyte additive engineering for aqueous Zn ion batteries. *Energy Storage Materials* **2022**, 51, 733-755. DOI: https://doi.org/10.1016/j.ensm.2022.07.017. (b) Mao, C.; Chang, Y.; Zhao, X.; Dong, X.; Geng, Y.; Zhang, N.; Dai, L.; Wu, X.; Wang, L.; He, Z. Functional carbon materials for high-performance Zn metal anodes. *Journal of Energy Chemistry* **2022**, 75, 135-153. DOI: https://doi.org/10.1016/j.jechem.2022.07.034.
- (21) Chuanfang; Park, S.-H.; O'Brien, S. E.; Seral-Ascaso, A.; Liang, M.; Hanlon, D.; Krishnan, D.; Crossley, A.; McEvoy, N.; Coleman, J. N.; et al. Liquid exfoliation of interlayer spacing-tunable 2D vanadium oxide nanosheets: High capacity and rate handling Li-ion battery cathodes. *Nano Energy* **2017**, *39*, 151-161. DOI: 10.1016/j.nanoen.2017.06.044.

- (22) (a) Abello, L.; Husson, E.; Repelin, Y.; Lucazeau, G. Structural study of gels of V2O5: Vibrational spectra of xerogels. *Journal of Solid State Chemistry* **1985**, *56* (3), 379-389. DOI: 10.1016/0022-4596(85)90188-4. (b) Avansi Jr, W.; Ribeiro, C.; Leite, E. R.; Mastelaro, V. R. Vanadium Pentoxide Nanostructures: An Effective Control of Morphology and Crystal Structure in Hydrothermal Conditions. *Crystal Growth & Design* **2009**, *9* (8), 3626-3631. DOI: 10.1021/cg900373f.
- (23) Ridley, P.; Gallano, C.; Andris, R.; Shuck, C. E.; Gogotsi, Y.; Pomerantseva, E. MXene-Derived Bilayered Vanadium Oxides with Enhanced Stability in Li-Ion Batteries. *ACS Applied Energy Materials* **2020**, *3* (11), 10892-10901. DOI: 10.1021/acsaem.0c01906.
- (24) Mansour, A.; Dallek, S.; Smith, P.; Baker, W. Thermogravimetry and X-Ray Absorption Spectroscopy Study of Heated V₂O₅·nH₂O Aerogels and Ambigels. *Journal of the Electrochemical Society* **2002**, *149* (12), A1589.
- (25) Wu, Q.-H.; Thissen, A.; Jaegermann, W.; Liu, M. Photoelectron spectroscopy study of oxygen vacancy on vanadium oxides surface. *Applied Surface Science* **2004**, *236* (1-4), 473-478.
- (26) Stich, M.; Göttlinger, M.; Kurniawan, M.; Schmidt, U.; Bund, A. Hydrolysis of LiPF₆ in Carbonate-Based Electrolytes for Lithium-Ion Batteries and in Aqueous Media. *The Journal of Physical Chemistry C* **2018**, *122* (16), 8836-8842. DOI: 10.1021/acs.jpcc.8b02080.
- (27) (a) Cohen, Y. S.; Aurbach, D. Surface films phenomena on vanadium-pentoxide cathodes for Li and Li-ion batteries: in situ AFM imaging. *Electrochemistry Communications* **2004**, *6* (6), 536-542. DOI: https://doi.org/10.1016/j.elecom.2004.03.014. (b) Moretti, A.; Jeong, S.; Passerini, S. Enhanced Cycling Ability of V2 O5 Aerogel using Room-Temperature Ionic Liquid-Based Electrolytes. *ChemElectroChem* **2016**, *3* (7), 1048-1053. DOI: 10.1002/celc.201600040.
- (28) Wangoh, L. W.; Huang, Y.; Jezorek, R. L.; Kehoe, A. B.; Watson, G. W.; Omenya, F.; Quackenbush, N. F.; Chernova, N. A.; Whittingham, M. S.; Piper, L. F. J. Correlating Lithium Hydroxyl Accumulation with Capacity Retention in V₂O₅ Aerogel Cathodes. *ACS Applied Materials & Interfaces* **2016**, *8* (18), 11532-11538. DOI: 10.1021/acsami.6b02759.
- (29) Moretti, A.; Passerini, S. Bilayered Nanostructured V₂O₅·nH₂O for Metal Batteries. *Advanced Energy Materials* **2016**, *6* (23), 1600868. DOI: https://doi.org/10.1002/aenm.201600868.